

PAPER

Structural and magnetic properties of $\text{Fe}_{1-x}\text{Co}_x\text{Se}_{1.09}$ nanoparticles obtained by thermal decomposition

To cite this article: Oksana A Li *et al* 2015 *Mater. Res. Express* **2** 126501

View the [article online](#) for updates and enhancements.

Related content

- [Magnetic and Mössbauer spectroscopy studies of hollow microcapsules made of silica-coated \$\text{CoFe}_2\text{O}_4\$ nanoparticles](#)
I S Lyubutin, N E Gervits, S S Starchikov et al.
- [Granular \$\text{Fe}_3\text{O}_4\$ - \$\text{CoO}\$ hetero-nanostructures produced by in situ seed mediated growth in polyol: magnetic properties and chemical stability](#)
R Sayed Hassan, T Gaudisson, N Yaacoub et al.
- [Origin of the magnetic transition at 100 K in \$\text{Fe}_2\text{O}_3\$ nanoparticles studied by x-ray absorption fine structure spectroscopy](#)
J López-Sánchez, A Muñoz-Noval, C Castellano et al.

INTERNATIONAL OPEN ACCESS WEEK
OCTOBER 19-26, 2020

ALL ECS ARTICLES. ALL FREE. ALL WEEK.
www.ecsdl.org

**NOW
AVAILABLE**

Materials Research Express



PAPER

Structural and magnetic properties of $\text{Fe}_{1-x}\text{Co}_x\text{Se}_{1.09}$ nanoparticles obtained by thermal decompositionOksana A Li^{1,2}, Chun-Rong Lin¹, Hung-Yi Chen¹, Hua-Shu Hsu¹, Kai-Wun Wu¹, Yaw-Teng Tseng¹, Oleg A Bayukov³, Irina S Edelman³, Sergey G Ovchinnikov^{2,3} and Kun-Yauh Shih⁴¹ Department of Applied Physics, National Pingtung University, Pingtung 90003, Taiwan² Siberian Federal University, Krasnoyarsk, 660041, Russia³ L. V. Kirensky Institute of Physics, SB RAS, Krasnoyarsk, 660036, Russia⁴ Department of Applied Chemistry, National Pingtung University, Pingtung 90003, TaiwanE-mail: crlin@mail.npue.edu.tw

Keywords: nanoparticles, chalcogenide, iron–cobalt selenide, ferrimagnetism, paramagnetism, Mössbauer spectroscopy

Abstract

A series of $\text{Fe}_{1-x}\text{Co}_x\text{Se}_{1.09}$ ($x = 0$ to 1) nanoparticles were synthesized by thermal decomposition method. Particles in composition range $\text{Fe}_{0.5}\text{Co}_{0.5}\text{Se}_{1.09}$ to $\text{CoSe}_{1.09}$ crystallized in monoclinic structure of $\text{Co}_{6,8}\text{Se}_8$, while $\text{FeSe}_{1.09}$ crystallized in hexagonal structure of FeSe achavalite. Magnetization dependences on temperature and external magnetic field reveal complicated magnetic behavior and correspond to the sum of paramagnetic and superparamagnetic response. Mössbauer spectra contain several paramagnetic doublets with parameters corresponding to nonequivalent positions of divalent and trivalent iron cations with low spin. The nonequivalent positions appeared due to inhomogeneous distribution of Co ions or metal vacancies in iron surrounding.

1. Introduction

Chalcogenide compounds attract great attention due to their useful semiconductor, photo-semiconductor, luminescent, scintillation, and recently discovered superconducting properties [1–7]. The structure and composition of the chalcogenide compounds strongly affect their magnetic properties [8, 9].

Iron selenide FeSe_y with $0.96 < y < 0.98$ (49.0–49.4 at% Se) has tetragonal PbO-structure [10] with Fe atoms occupying two-dimensional square layers within cubic close-packed Se lattice. Each Fe atom is surrounded by four Se atoms forming distorted FeSe_4 tetrahedra [11]. Crystal structure of iron selenide FeSe_y with $1 < y < 1.25$ is based on NiAs unit cell, where Fe cation occurs in octahedral coordination created by six Se, and Se anion occurs in trigonal prismatic arrangement, created by six Fe cations [12]. This structure omits metal atoms thus creating iron vacancies. An ordered distribution of vacancies forms a superlattice nC which is n times larger than the unit NiAs subcell in the 'C' direction. FeSe_y can have monoclinic ($\sim\text{Fe}_3\text{Se}_4$) or hexagonal ($\sim\text{Fe}_7\text{Se}_8$) symmetry. According to P Terzieff *et al* [13], hexagonal FeSe_y exhibits antiferromagnetism at compositions $\text{FeSe}_{1.02}$ – $\text{FeSe}_{1.11}$ (50.5–52.5 at% Se) and ferrimagnetism at compositions $\text{FeSe}_{1.11}$ – $\text{FeSe}_{1.19}$ (52.5–54.3 at% Se) with Curie temperature about $T_C \approx 450$ K. For antiferromagnetic alloys P Terzieff *et al* [13] observed the transition to the paramagnetic state in the unstable range between room temperature and 573 K.

Crystal structure of cobalt selenide CoSe_y ($1 < y < 1.20$) is hexagonal of the NiAs-like type. At composition $\text{CoSe}_{1.20}$, a lowering of symmetry from hexagonal to monoclinic occurs [14]. At compositions $\text{CoSe}_{1.03}$ – $\text{CoSe}_{1.14}$, distribution of Co atoms and vacancies forms the stacking of Kagomé net-like planes and fully occupied NiAs-like planes along the c -axis. At compositions $\text{CoSe}_{1.14}$ – $\text{CoSe}_{1.25}$, the AFCFA superstructure of the Cr_7Se_8 -type is formed, where 'A' and 'C' are Kagomé nets and 'F' is fully occupied layer [15]. CoSe_y with $1.05 < y < 1.20$ exhibits ferrimagnetism while CoSe_y with $y > 1.20$ is paramagnetic according to Bohm *et al* [14]. But according to M. Sato *et al* [16] and T Kamimura [17], Co_7Se_8 ($y \approx 1.14$) is paramagnetic and $(\text{Fe}_{1-x}\text{Co}_x)_7\text{Se}_8$ exhibit ferrimagnetism at $x < 0.6$ with Curie temperature varying from $T_C \approx 450$ K for Fe_7Se_8 to $T_C \approx 80$ K for $(\text{Fe}_{0.43}\text{Co}_{0.57})_7\text{Se}_8$.

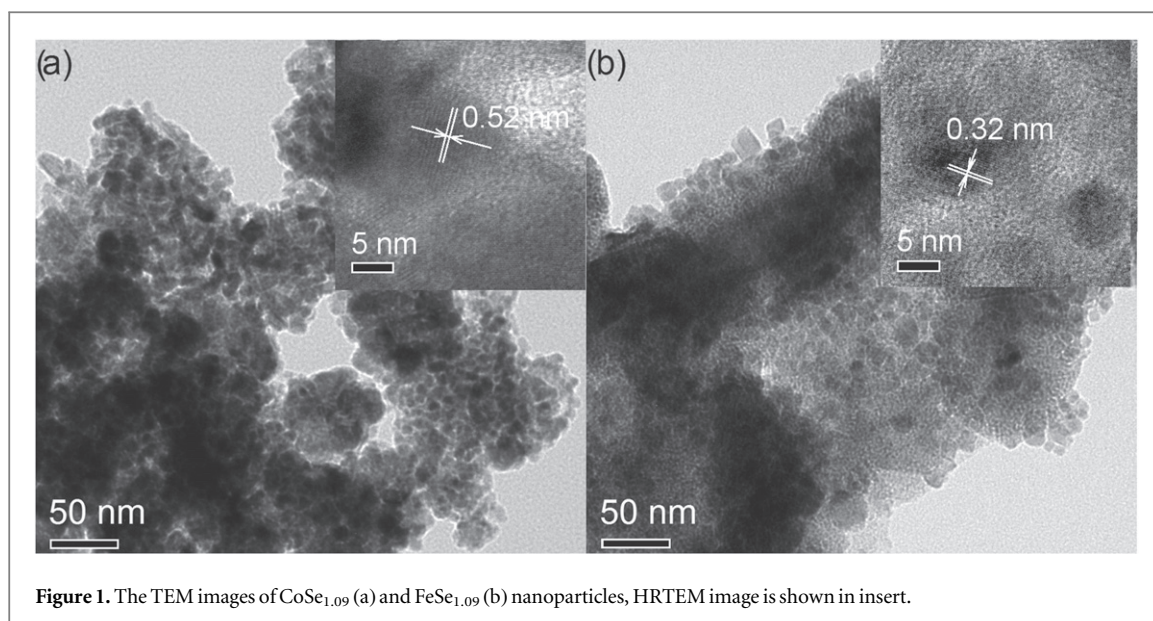


Figure 1. The TEM images of CoSe_{1.09} (a) and FeSe_{1.09} (b) nanoparticles, HRTEM image is shown in insert.

Basing on the data presented, the possibility can be supposed of the different magnetic phases coexistence in the same sample. The present paper is aimed at finding of such states in the system Fe_{1-x}Co_xSe_{1.09}. The specified Se concentration was chosen because FeSe_y and CoSe_y demonstrate different magnetic states for $y = 1.09$: antiferromagnetic and ferrimagnetic, respectively, as it was mentioned above.

2. Experiment

A series of powdered Fe_{1-x}Co_xSe_{1.09} ($x = 0$ to 1) samples was synthesized by the method of thermal decomposition of the source components in high-temperature solutions in a three-neck flask equipped with an inlet of argon gas, condenser, magnetic stirrer, thermocouple, and heating mantle. Iron(III) nitrate Fe(NO₃)₃, cobalt nitrate Co(NO₃)₂ and selenium Se in an appropriate ratio, oleylamine and oleic acid were put into the three-neck flask, heated up to 180 °C and kept for 30 min under this temperature in argon gas. Then the mixture was heated up to 200 °C for 1 h to decompose salts, after that the mixture was heated up to 350 °C. The synthesized powder was cooled to room temperature and washed thoroughly with hexane.

The morphology of the particles was examined by the transmission electron microscope (TEM, Tecnai G2 F20, FEG-TEM, Philips Co. Ltd). The crystal structure and phase purity of the samples were examined by x-ray powder diffraction (XRD) with the use of a Mutiflex MF2100, Rigaku Co. Ltd diffractometer equipped with a Cu K α radiation source in the 2θ range of 10°–80° with a step size of 0.02°. Magnetic properties were analyzed using a SQUID magnetometer. Temperature dependences of magnetization were measured at temperatures between 5 and 390 K in an applied field of 100 Oe. The measurements of hysteresis loops were carried out at 5, 120, and 300 K in an applied field sweeping from –50 to 50 kOe. Mössbauer measurements were performed on MS-1104Em spectrometer at room temperature. Co⁵⁷ (Cr) radiation source was used. Powders had density of 5–10 mg cm⁻².

3. Results and discussion

The TEM images of the CoSe_{1.09} and FeSe_{1.09} nanoparticles are shown in figure 1. The agglomerates of spherical CoSe_{1.09} nanoparticles are observed in the figure 1(a). The insert shows high resolution TEM (HRTEM) image, one can see a lattice fringe spacing of 0.52 nm, which represents the (001) planes of the monoclinic Co_{6.8}Se₈. In figure 1(b) FeSe_{1.09} nanoparticles of spherical, cubic or irregular forms are observed. The HRTEM image in insert shows the nanoparticle with lattice fringe spacing of 0.32 nm, which represents the (100) planes of the hexagonal achavalite.

TEM images were used to plot diagrams of particle size distribution (bar-graphs in figures 2(a) and (b)). The particle size distribution of nanocrystalline materials is usually described by log-normal function[18]:

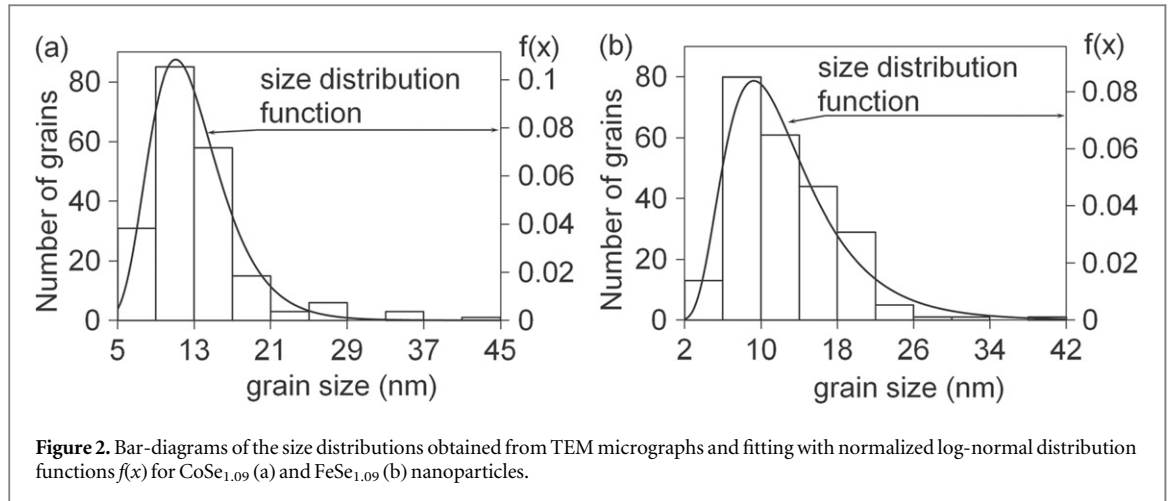


Figure 2. Bar-diagrams of the size distributions obtained from TEM micrographs and fitting with normalized log-normal distribution functions $f(x)$ for $\text{CoSe}_{1.09}$ (a) and $\text{FeSe}_{1.09}$ (b) nanoparticles.

$$f(x) = \frac{1}{x\sigma\sqrt{2\pi}} \exp\left(-\frac{[\ln(x/d_0)]^2}{2\sigma^2}\right), \quad (1)$$

here x is the particle size, d_0 is the median of the size distribution function.

The arithmetic mean d_{num} , and variance $\text{Var}(x)$ are:

$$d_{\text{num}} = d_0 \exp\left(\frac{\sigma^2}{2}\right), \quad (2)$$

$$\text{Var}(x) = \left(\exp(\sigma^2) - 1\right)d_0^2 \exp(\sigma^2). \quad (3)$$

The standard deviation of the log-normal size distribution is the square root of the variance.

Approximation of data received from TEM images by function (1) let us determine d_0 and σ . The arithmetic mean d_{num} and standard deviation were found from equations (2) and (3) to be 12.9 and 4.2 nm for $\text{CoSe}_{1.09}$ and 12.8 and 6.2 nm for $\text{FeSe}_{1.09}$. $\text{CoSe}_{1.09}$ particles have narrower size distribution in comparison with $\text{FeSe}_{1.09}$.

The volume-weighted average grain size d_{vol} can be found as [19]:

$$d_{\text{vol}} = d_0 \exp\left(\frac{7\sigma^2}{2}\right). \quad (4)$$

The volume-weighted average grain size d_{vol} was found to be 17.4 nm for $\text{CoSe}_{1.09}$ and 24.2 nm for $\text{FeSe}_{1.09}$, respectively.

The XRD analysis of $\text{Fe}_{1-x}\text{Co}_x\text{Se}_{1.09}$ ($x = 0-1$) samples showed (figure 3) that the observed peak positions and intensities are in good agreement with the database provided by Match2 software, card (96-901-2807) for $\text{Co}_{6.8}\text{Se}_8$, which has a monoclinic structure with a space group of $C 1 2/m 1$ (for samples with $x = 0.5-1$), and card (96-101-1367) for FeSe achavalite, which has a hexagonal structure with a space group $P6_3/mmc$ (for sample with $x = 0$).

The average crystallite size varies from 12 ($x = 0.58$) to 26 ($x = 0$) nm (table 1) as estimated by Scherrer's formula:

$$d = K\lambda/\Delta(2\theta)\cos\theta. \quad (5)$$

Here d is the volume-weighted average size of crystallites, K is the dimensionless shape factor assumed to be 0.94, $\lambda = 0.15406$ nm is the wavelength for the $\text{Cu K}\alpha$ radiation source, θ is the Bragg angle and $\Delta(2\theta)$ is the full width of the diffraction peak at half maximum located at 2θ . The most intensive diffraction peak was chosen, it is the peak of (101) crystal plane ($2\theta = 32.42^\circ$) for FeSe and the peak of (220) crystal plane for $\text{Fe}_{1-x}\text{Co}_x\text{Se}_{1.09}$ ($x = 0.5-1$) samples ($2\theta = 33.54^\circ$ for $\text{Co}_{6.8}\text{Se}_8$). The calculated d values are in a good agreement with volume-weighted average grain size d_{vol} determined from TEM images.

The magnetization curves measured in an applied magnetic field up to 50 kOe are shown in figure 4. The low temperature magnetization curves are very similar in shape for all x values: hysteresis is in relatively low fields and, practically, linear dependence on magnetic field is observed, when it exceeds ~ 20 kOe. Magnetic saturation is not reached even at $H = 50$ kOe. A step increase of the magnetization in the maximal magnetic field used as well as of the coercivity value, H_c , are observed when x changes from 1.0 to 0.5. With the temperature increase from 5 to 300 K, the shape of the magnetization curve in the low field region changes noticeably: H_c reduces

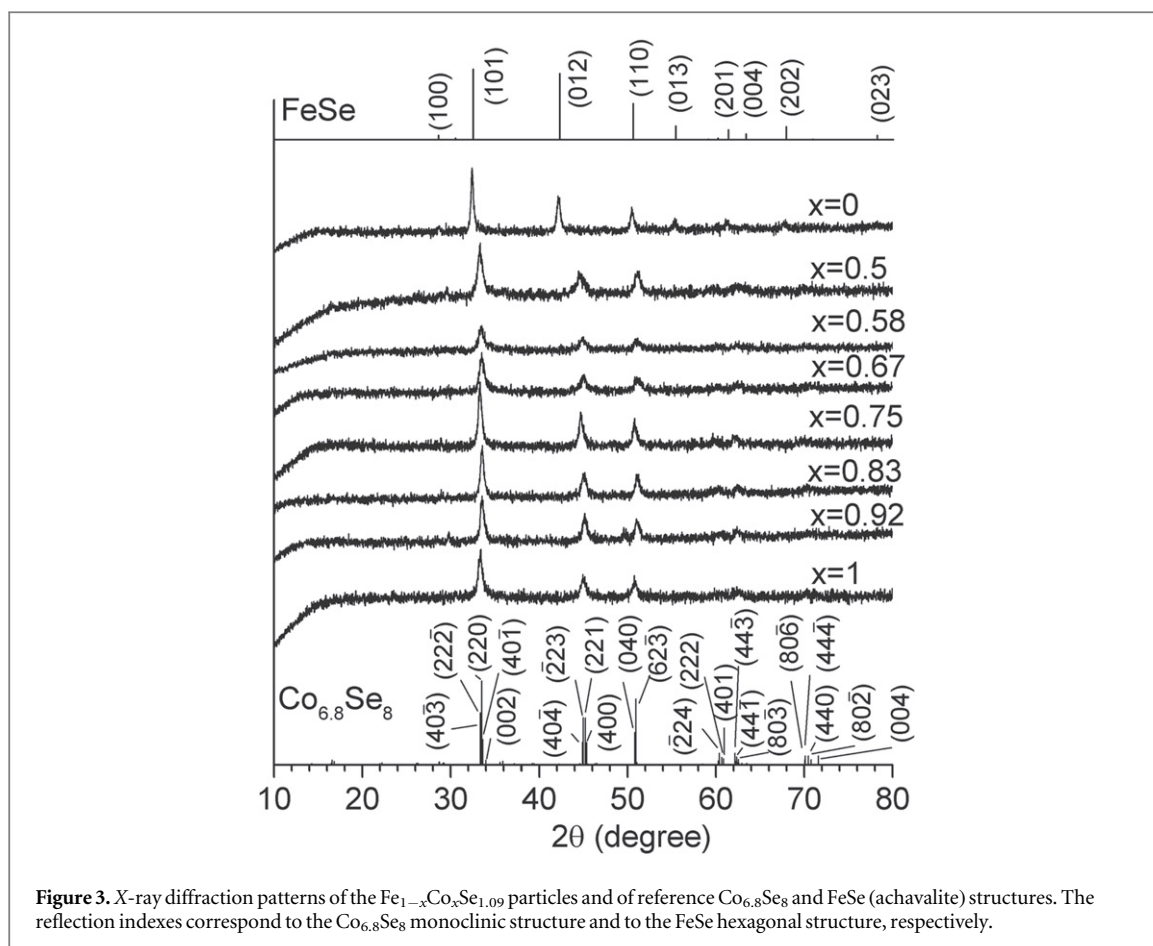


Figure 3. X-ray diffraction patterns of the $\text{Fe}_{1-x}\text{Co}_x\text{Se}_{1.09}$ particles and of reference $\text{Co}_{6.8}\text{Se}_8$ and FeSe (achavalite) structures. The reflection indexes correspond to the $\text{Co}_{6.8}\text{Se}_8$ monoclinic structure and to the FeSe hexagonal structure, respectively.

Table 1. Average crystallite size of $\text{Fe}_{1-x}\text{Co}_x\text{Se}_{1.09}$.

X	1	0.92	0.83	0.75	0.67	0.58	0.5	0
Crystallite size d , nm	15	17	18	19	14	12	17	26

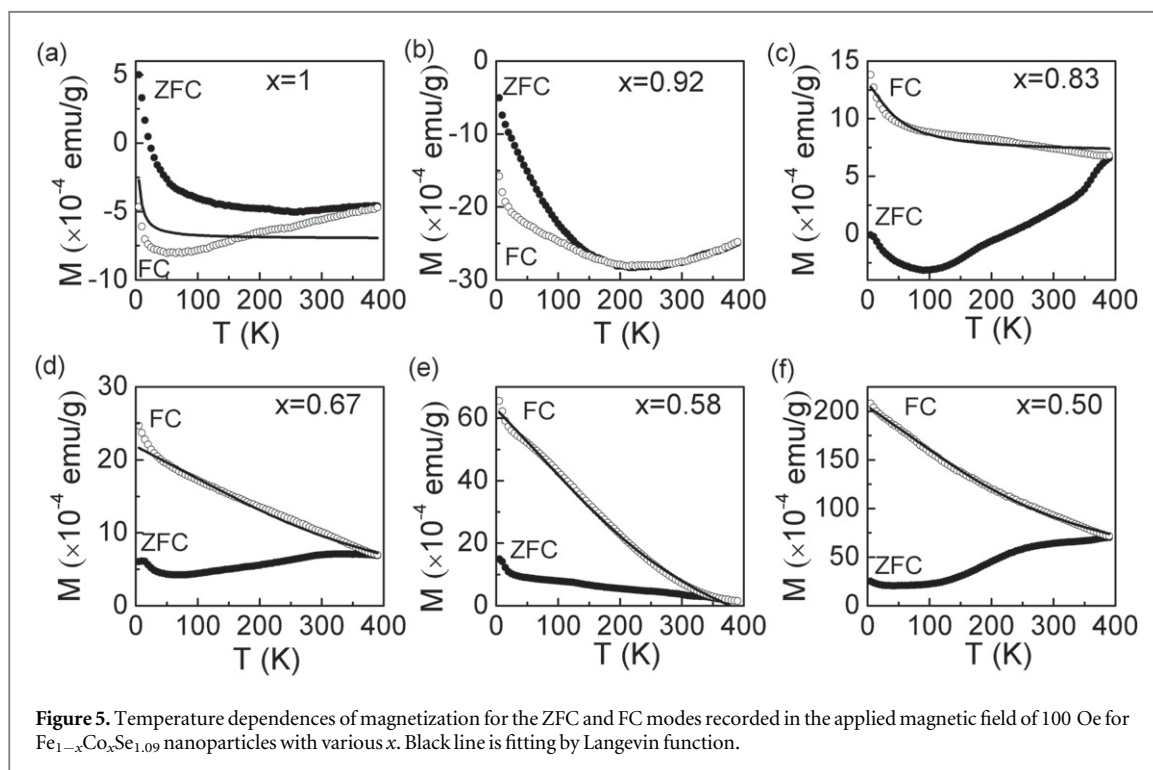
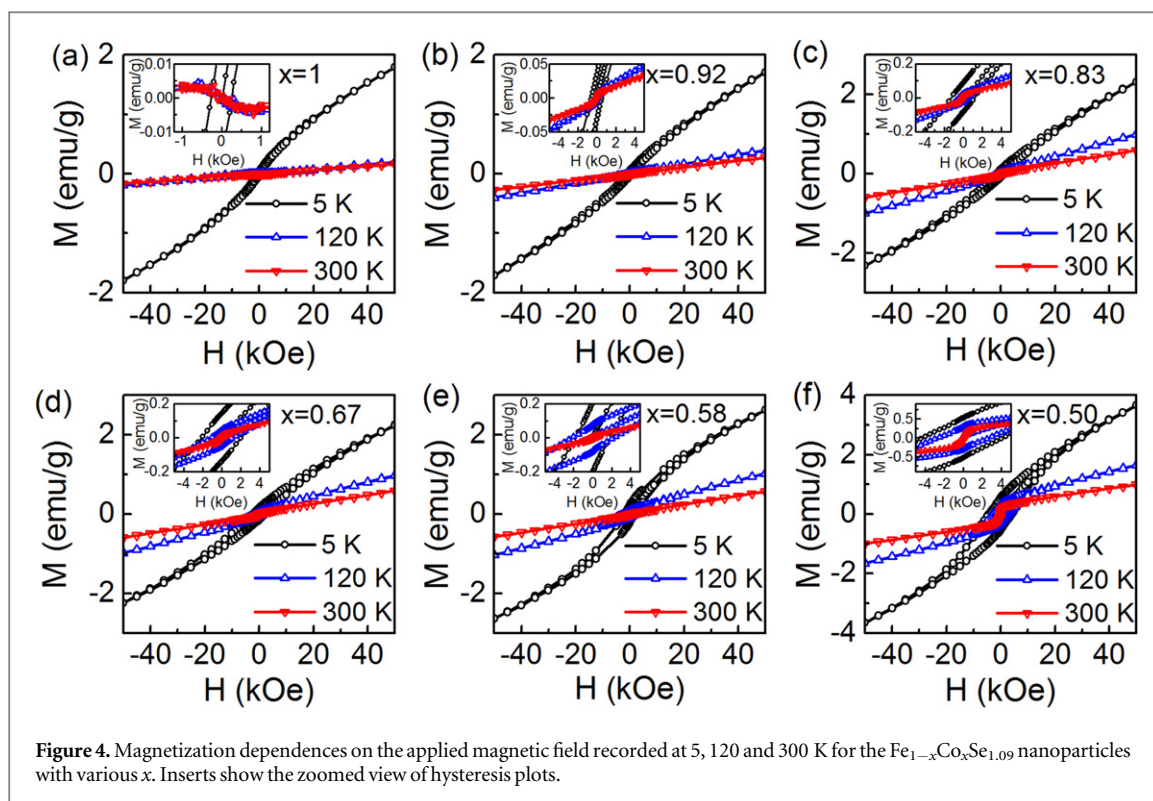
significantly in all samples and hysteresis disappears at 120 K for $x = 0.83$ to 1 and at 300 K for $x = 0.5$ to 0.67. However, the bend in low field curves for ferro- or ferrimagnetic states remains at higher temperatures, both at 120 and 300 K. The bend is absent, practically, for samples with $x = 0.58$ and 0.67 containing nanoparticles of the lowest average diameter. All these facts can evidence the coexistence of the paramagnetic nanoparticles (or diluted paramagnetic ions) and superparamagnetic nanoparticles. The assumption of strong paramagnetic contribution at low temperatures is in a good agreement with literature data [16, 17] according to which pseudo-binary systems $(\text{Fe}_{1-x}\text{Co}_x)_7\text{Se}_8$ exhibit paramagnetism for $x = 0.6$ –1. Part of superparamagnetic nanoparticles is ‘frozen’ at low temperature providing hysteresis. Opposite sign of magnetization in the region of bend at 120 and 300 K should be noted for sample with $x = 1$.

The temperature dependences of magnetization recorded in zero-field-cooled (ZFC) and field-cooled (FC) regimes in an applied field of 100 Oe are shown in figure 5. The difference between FC and ZFC curves is characteristic for the magnetically inhomogeneous systems such as ensembles of superparamagnetic particles. The pictures for samples with x from 0.83 to 0.50 are typical for such systems confirming the idea mentioned above on the superparamagnetic contribution to the magnetization curves.

The FC magnetization dependence for $x = 0.5$ (figure 5(f)) obeys the Langevin functional equation for paramagnetic and superparamagnetic particles:

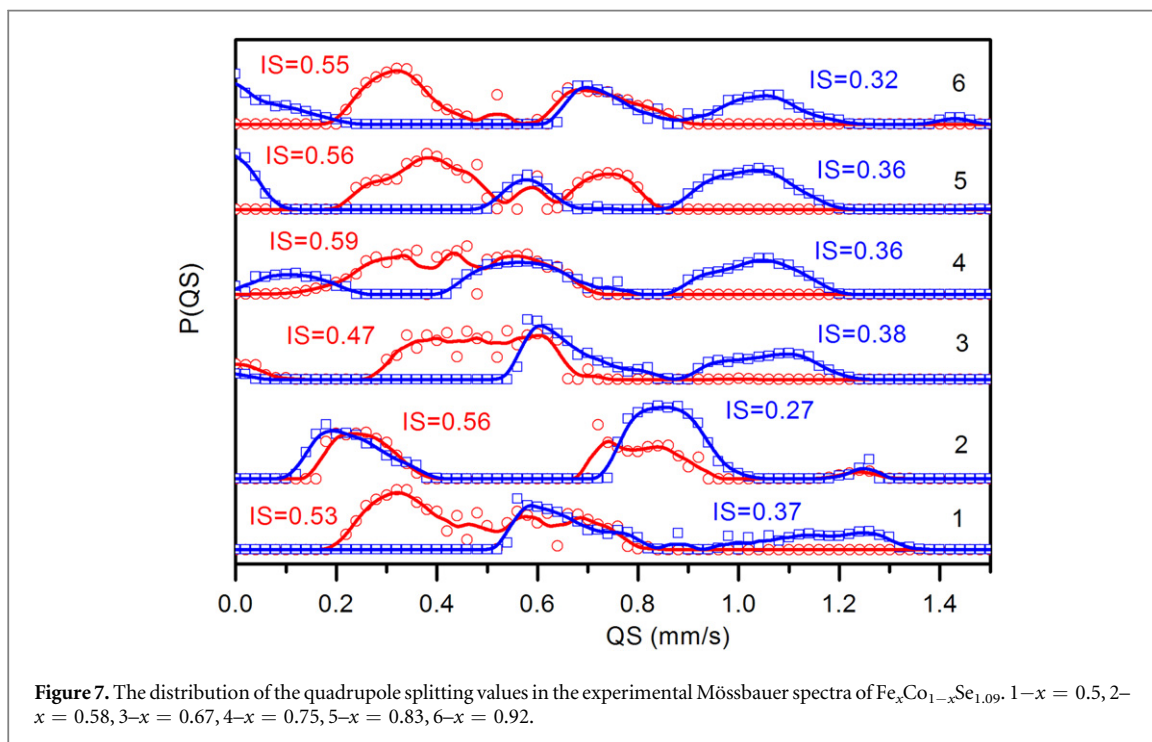
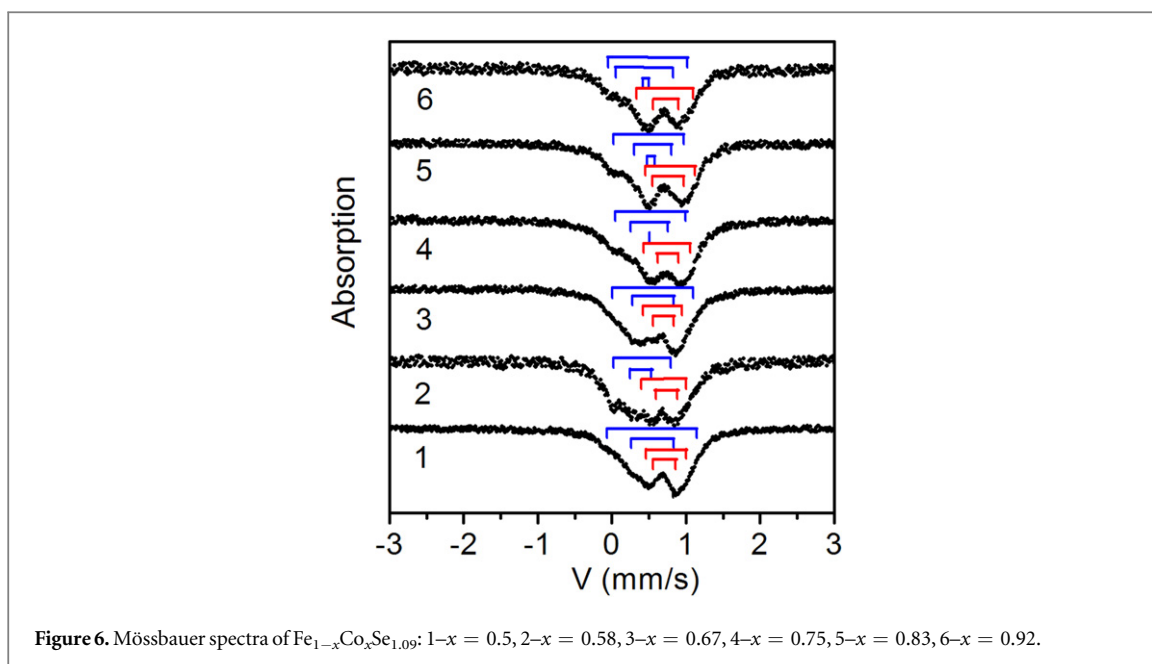
$$M(T) = n\mu_* \text{cth}(H\mu/kT) - kT/H\mu. \quad (6)$$

Here k is Boltzmann constant, μ —magnetic moment, n —number of particles with magnetic moment μ , per 1 g. The value of μ and n are found from fitting to be $n = 3.2 \times 10^{14} \text{ g}^{-1}$, $\mu = 6.9 \times 10^4 \mu_b$, here $\mu_b = 9.27 \times 10^{-21} \text{ Erg/G}$ is Bohr magneton. This result can be due to superparamagnetism of $\text{Fe}_{0.5}\text{Co}_{0.5}\text{Se}_{1.09}$ sample. Hence one can estimate the diameter of superparamagnetic particles to be $d = (6/\pi n\rho)^{1/3} \approx 92 \text{ nm}$,



taking into account that the density of $\text{Fe}_{0.5}\text{Co}_{0.5}\text{Se}_{1.09}$ is of the same order that density of Co_7Se_8 $\rho = 7.54 \text{ g cm}^{-3}$ [15]. This result however disagrees with TEM and XRD data.

The more complicated case takes place for samples with $x = 1.0$ and 0.92 when magnetization direction is opposite to the external magnetic field (figures 5(a) and (b), respectively). Such a behavior may originate from the biasing field, as it happens, for example, in ferromagnetic/antiferromagnetic structures. As the used technology cannot exclude a Co oxidation process and antiferromagnetic CoO inclusions inside or in the surface of nanoparticles, the interaction between CoO and CoSe can cause the opposite magnetization direction in low magnetic field.

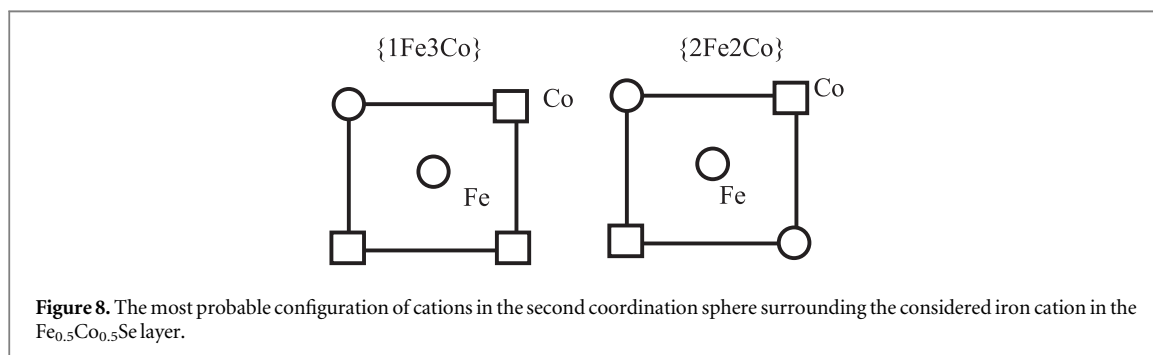


Room temperature Mössbauer spectra are shown in figure 6. It can be seen that the spectra are composed of the sum of quadrupole doublets with different chemical shifts.

Interpretation of the spectra has been carried out in two stages. As a first step, the distribution of quadrupole splitting $P(QS)$ values in the experimental spectra was defined, figure 7. For this purpose, two groups of doublets with different chemical shifts (IS) were used. The IS value was the same inside each group. The IS value and the amplitude of the doublets were fitted to the experimental curves. As a result, for each sample two distributions $P(QS)$ were received: for relatively high value of chemical shift ($IS = 0.52\text{--}0.59 \text{ mm s}^{-1}$ —red circles) and for low value of chemical shift ($IS = 0.27\text{--}0.36 \text{ mm s}^{-1}$ —blue squares). Maxima in the distributions $P(QS)$ indicate possible nonequivalent positions of iron in the investigated selenides. Positions can be considered as possible but not veritable one's because at fitting we used chemical shifts that are common for each group of doublets. Number of maxima of $P(QS)$ corresponds to the number of non-equivalent positions, coordinate on the QS axis corresponds to the splitting of possible doublets, the intensity of maxima corresponds to the approximate population of the position.

Table 2. Mössbauer parameters of $\text{Fe}_x\text{Co}_{1-x}\text{Se}_{1.09}$ selenide. IS— isomer chemical shift with respect to $\alpha\text{-Fe}$, QS—quadrupole splitting, Γ —width of the absorption line A—the area under partial doublet (the population of the position).

X	IS \pm 0.005 mm s ⁻¹	QS \pm 0.02 mm s ⁻¹	Γ \pm 0.02 mm s ⁻¹	A \pm 0.05	Position
0.5	0.558	0.31	0.21	0.15	Fe ³⁺ (6)LS
	0.580	0.55	0.24	0.20	
	0.395	0.57	0.42	0.54	Fe ²⁺ (4)LS or Fe ²⁺ (6)LS
	0.383	1.20	0.29	0.11	
0.58	0.579	0.29	0.12	0.04	Fe ³⁺ (6)LS
	0.546	0.62	0.38	0.40	
	0.238	0.29	0.23	0.15	Fe ²⁺ (4)LS or Fe ²⁺ (6)LS
	0.247	0.77	0.32	0.41	
0.67	0.545	0.27	0.18	0.09	Fe ³⁺ (6)LS
	0.527	0.52	0.17	0.06	
	0.408	0.56	0.49	0.77	Fe ²⁺ (4)LS or Fe ²⁺ (6)LS
	0.387	1.10	0.24	0.08	
0.75	0.598	0.29	0.25	0.23	Fe ³⁺ (6)LS
	0.585	0.63	0.24	0.19	
	0.358	0.01	0.21	0.07	Fe ²⁺ (4)LS or Fe ²⁺ (6)LS
	0.346	0.50	0.19	0.08	
	0.359	0.95	0.51	0.44	
0.83	0.598	0.423	0.26	0.21	Fe ³⁺ (6)LS
	0.625	0.659	0.24	0.16	
	0.375	0.108	0.15	0.06	Fe ²⁺ (4)LS or Fe ²⁺ (6)LS
	0.396	0.498	0.29	0.21	
	0.336	0.942	0.41	0.36	
0.92	0.574	0.33	0.24	0.24	Fe ³⁺ (6)LS
	0.556	0.75	0.26	0.22	
	0.302	0.08	0.21	0.06	Fe ²⁺ (4)LS or Fe ²⁺ (6)LS
	0.282	0.76	0.47	0.42	
	0.328	1.05	0.31	0.05	



In the second stage of the spectra interpretation, the model spectrum was formed based on the information about P(QS), which was fitted to the experimental spectrum. With this fitting false doublets vanish, and for the true doublets Mössbauer parameters are refined. The result of the second stage is shown in table 2.

Table 2 shows that each sample's spectrum contains two kinds of doublets different in chemical shift value $\sim 0.5\text{-}0.6$ mm s⁻¹ and ~ 0.3 mm s⁻¹. When comparing with the published data for iron chalcogenides [20], doublets with a large chemical shift value (IS = 0.54-0.67 mm s⁻¹) should be attributed to the low-spin (LS) Fe³⁺ cations in octahedral coordination of selenium, Fe³⁺(6Se). Some increase of the chemical shift value (up to 0.625) in our case is due, possibly, to changes in ion-ion distances when iron is substituted by cobalt. The presence of two doublets Fe³⁺(6Se) is also can be associated with a cationic substitution. It is illustrated by figure 8, which shows the two most probable configurations of cations that surround the considered Fe³⁺ cation in the second coordination sphere at the condition of the inhomogeneous distribution of the replacing Co ions. Local symmetry at this cation disposition in the configuration {1Fe3Co} is higher than in the configuration {2Fe2Co}. The quadrupole splitting QS, which characterizes the degree of distortion, for Fe in the first configuration should be less. The presence of two doublets Fe³⁺(6Se) can be associated also with vacancies in the second coordination sphere of the considered Fe³⁺ cation effecting in a decrease of symmetry of its nearest surrounding. The quadrupole splitting QS, which characterizes the degree of nearest surrounding distortion should be higher.

Mössbauer parameters of the quadrupole doublets with smaller values of chemical shifts are typical for low spin (LS) Fe^{2+} cations in iron chalcogenides with octahedral ($IS = 0.27\text{--}0.44 \text{ mm s}^{-1}$) [21–27] and tetrahedral ($IS = 0.3\text{--}0.51 \text{ mm s}^{-1}$) [7, 25–30] coordinations. Thus, the position of the iron with isomeric chemical shifts $IS = 0.5\text{--}0.6 \text{ mm s}^{-1}$ can be attributed to cations occupying the layers in the octahedral structure FeSe. These cations are trivalent and have low spin, indicated in the table by red color. Position (indicated by blue color) having a small chemical shift belong to phase with divalent iron ions with low spin. As far as XRD measurements didn't show tetrahedral structure, this phase is probably of distorted hexagonal type.

4. Conclusion

Summarizing results obtained, we have revealed complicated magnetic behavior in series of nanosized particles $\text{Fe}_{1-x}\text{Co}_x\text{Se}_{1.09}$ in dependence on the relative Co and Fe concentrations. Superparamagnetic state of $\text{Fe}_{0.5}\text{Co}_{0.5}\text{Se}_{1.09}$ powder with average particle size of 17 nm is shown. Mössbauer study showed nonequivalent positions of iron ions appearing due to the inhomogeneous distribution of Co ions or presence of metal vacancies in the second coordination sphere of iron ions.

Acknowledgments

This work is supported by the Ministry of Science and Technology of Taiwan (MOST 103-2811-M-153 -001 and MOST 102-2112-M-153 -002 -MY3).

References

- [1] Mizuguchi Y, Tomioka F, Tsuda S, Yamaguchi T and Takano Y 2008 Superconductivity at 27 K in tetragonal FeSe under high pressure *Appl. Phys. Lett.* **93** 152505
- [2] Hsu F-C et al 2008 Superconductivity in the PbO-type structure alpha-FeSe *Proc. Natl Acad. Sci. USA.* **105** 14262–4
- [3] Ozaki T, Deguchi K, Mizuguchi Y, Kawasaki Y, Tanaka T, Yamaguchi T, Kumakura H and Takano Y 2012 Fabrication of binary FeSe superconducting wires by diffusion process *J. Appl. Phys.* **111** 112620
- [4] Ozaki T et al 2012 Enhancement of superconducting properties in FeSe wires using a quenching technique *J. Appl. Phys.* **111** 013912
- [5] Chen T-K et al 2014 Fe-vacancy order and superconductivity in tetragonal $\beta\text{-Fe}_{1-x}\text{Se}$ *Proc. Natl Acad. Sci. USA.* **111** 63–8
- [6] Ge J, Liu Z-L, Liu C, Gao C, Qian D, Xue Q, Liu Y and Jia J-F 2014 Superconductivity above 100 K in single-layer FeSe films on doped SrTiO_3 *Nat. Mater.* **14** 285–9
- [7] Greenfield J T, Kamali S, Lee K and Kovnir K 2015 A solution for solution-produced $\beta\text{-FeSe}$: elucidating and overcoming factors that prevent superconductivity *Chem. Mater.* **27** 588–96
- [8] Lin C-R, Siao Y-J, Lu S-Z and Gau C 2009 Magnetic properties of iron selenide nanocrystals synthesized by the thermal decomposition *IEEE Trans. Magn.* **45** 4275–8
- [9] Lyubutin I S, Lin C-R, Funtov K O, Dmitrieva T V, Starchikov S S, Siao Y-J and Chen M-L 2014 Structural, magnetic, and electronic properties of iron selenide $\text{Fe}_6\text{-7Se}_8$ nanoparticles obtained by thermal decomposition in high-temperature organic solvents *J. Chem. Phys.* **141** 044704
- [10] Kubaschewski-von Goldbeck O 1982 *IRON—Binary Phase Diagrams* (Berlin: Springer)
- [11] Tsuji T, Howe A T and Greenwood N N 1976 The Fe–Se system. I. Mössbauer spectra and electrical conductivity of $\text{Fe}_{1.04}\text{Se}$ *J. Solid State Chem.* **17** 157–63
- [12] Wold A and Dwight K 1993 *Solid State Chemistry: Synthesis, Structure, and Properties of Selected Oxides and Sulfides* (Dordrecht: Springer Netherlands)
- [13] Terzieff P and Komarek K L 1978 The antiferromagnetic and ferrimagnetic properties of iron selenides with NiAs-type structure *Monatshfte fur Chemie* **109** 1037–47
- [14] Bohm F, Gronvold F, Haraldsen H and Prydz H 1955 X-ray and magnetic study of the system cobalt selenium *Acta Chem. Scand.* **9** 1510–22
- [15] García-García F J, Larsson A-K, Norèn L and Withers R L 2004 The crystal structures of Co_3Se_4 and Co_7Se_8 *Solid State Sci.* **6** 725–33
- [16] Sato M, Kamimura T and Iwata T 1985 Magnetic properties and anisotropy of $(\text{Fe}_{1-x}\text{Co}_x)_7\text{Se}_8$ *J. Appl. Phys.* **57** 3244
- [17] Kamimura T 1988 Correlation between magnetism and lattice spacing c in compounds with NiAs-type structures *Le J. Phys. Colloq.* **49** C8 191–C8 192
- [18] Gubicza J, Szépvölgyi J, Mohai I, Zsoldos L and Ungár T 2000 Particle size distribution and dislocation density determined by high resolution x-ray diffraction in nanocrystalline silicon nitride powders *Mater. Sci. Eng. A* **280** 263–9
- [19] Kril C E and Birringer R 1998 Estimating grain-size distributions in nanocrystalline materials from x-ray diffraction profile analysis *Philos. Mag. A* **77** 621–40
- [20] Bensch W, Helmer O, Lu J, Hesse H-J, Wortmann G, Kraus M and Luders K 1995 Crystal structures, chemical reactivity, magnetic properties, and Mössbauer spectroscopy of the quasi-ternary channel compounds $\text{TlV}_{5-y}\text{Fe}_y\text{S}_8$ ($y = 0.5\text{--}1.5$) *J. Solid State Chem.* **119** 147–56
- [21] Kjekshus A and Nicholson D G 1971 The significance of pi back-bonding in compounds with pyrite, marcasite, and arsenopyrite type structures *Acta Chem. Scand.* **25** 866–76
- [22] Temperley A A and Lefevre H W 1966 The Mössbauer effect in marcasite iron compounds* *J. Phys. Chem. Solids* **27** 85–92
- [23] Xie Y, Zhu L, Jiang X, Lu J, Zheng X, He W and Li Y 2001 Mild Hydrothermal-reduction synthesis and Mössbauer study of low-dimensional iron chalcogenide microcrystals and single crystals *Chem. Mater.* **13** 3927
- [24] Nishihara Y and Ogawa S 1979 Mössbauer study of ^{57}Fe in the pyrite-type dichalcogenides *J. Chem. Phys.* **71** 3796–801

- [25] Campos C E M, de Lima J C, Grandi T A, Machado K D, Drago V and Pizani P S 2004 XRD, DSC, MS and RS studies of Fe₇₅Se₂₅ iron selenide prepared by mechano-synthesis *J. Magn. Magn. Mater.* **270** 89–98
- [26] Campos C E M, Drago V, de Lima J C, Grandi T A, Machado K D and Silva M R 2004 Mössbauer and magnetization studies of Fe₂₅Se₇₅ iron selenides produced by mechanical alloying *J. Magn. Magn. Mater.* **269** 6–14
- [27] Reddy K V and Chetty S C 1975 Mossbauer Studies on the Fe–Te system *Phys. Status Solidi* **37** 687
- [28] Hamdeh H H, El-Tabey M M, Asmatulu R, Ho J C, Huang T W, Yeh K W and Wu M K 2010 Mössbauer spectroscopy of spin dynamics in Mn_xFe_{1-x}Se_{0.85} superconductors: evidence for an incommensurate-spin-density-wave state *Europhys. Lett.* **89** 67009
- [29] McQueen T M et al 2009 Extreme sensitivity of superconductivity to stoichiometry in Fe_{1+δ}Se *Phys. Rev. B* **79** 014522
- [30] Gómez R W, Marquina V, Pérez-Mazariego J L, Escamilla R, Escudero R, Quintana M, Hernández-Gómez J J, Ridaura R and Marquina M L 2010 Effects of substituting Se with Te in the FeSe compound: structural, magnetization and Mössbauer studies *J. Supercond. Nov. Magn.* **23** 551–7